

Electronic Supplementary Information

Superior performance of borocarbonitrides, $B_xC_yN_z$, as stable, metal-free electrocatalysts for hydrogen evolution reaction.

Manjeet Chhetri^a, Somak Maitra^a, Himanshu Chakraborty^b, Umesh Waghmare^b, C. N. R. Rao^{*a}

^a New Chemistry Unit, International Centre for Materials Science, Jawaharlal Nehru Centre for Advanced Scientific Research, P.O Jakkur, Bangalore, 560064, India. Email: cnrrao@jncasr.ac.in

^b Theoretical Sciences Unit, Jawaharlal Nehru Centre for Advanced Scientific Research, P.O Jakkur, Bangalore 560064, India.

Experimental Section:

Chemicals: Urea, Boric acid and Activated charcoal were purchased from SD Fine Chemicals, India. Nafion (perfluorosulfonic acid cation exchange polymer; 5 wt% in aliphatic alcohols) solution was a bought from Sigma Aldrich. 40% commercial Pt/C catalyst was purchased from Sigma Aldrich and used for comparison purpose. Absolute ethanol (HPLC grade) and Sulphuric acid (H_2SO_4 , analytical grade) were obtained from SD Fine Chemicals, India. All the chemicals were used as it is without further purification.

Synthesis of $B_xC_yN_z$: Synthesis was carried out by a urea method as reported earlier by our group¹. Briefly, required amounts of boric acid, urea and activated charcoal were mixed step by step ensuring full solubility of boric acid and urea in 20 mL DI water. Then the proportionate mixture was ultrasonicated (Elmasonic P 30H model, 37 kHz, 100% power) for 20 minutes to obtain a homogeneous dispersion which was heated at 80°C. When a slurry was obtained as a result of evaporation of the solvent, it was transferred into a quartz boat and heated in a tubular furnace at 900°C for 10 h under N_2 atmosphere (heating rate=4°C/min). Then subsequently the obtained black sample was treated with NH_3 at 900°C for 4 h (heating rate=4°C/min). 5 different compositions of BCN nanosheets were obtained by varying the initial amount of B, N and C precursor viz. boric acid, urea, activated charcoal respectively.

Materials Characterizations: The morphology of the obtained BCN nanosheets were studied by Transmission electron microscopy (TEM, Technai F30 UHR, 200 kV) . The atomic ratio of the elements and the corresponding elemental composition of the samples were studied by XPS measurements, carried out with an Omicron spectrometer using Al Ka as the X-ray source (1486.6 eV), Perkin–Elmer 2400 CHN analyzer and FEI Quanta FESEM equipped with energy dispersive X-ray spectroscopy (EDX), under 10 kV accelerating voltage and 10 microsecond accumulation time. Surface area measurements were carried out with a Quanta Chrome Autosorb- 1 instrument. Powder X-ray diffraction (XRD) patterns of the reaction products were recorded using a Bruker Diffractometer with Cu K α radiation (D8 Advance X-ray diffractometer, Cu K α , $\lambda = 1.5406 \text{ \AA}$, 40 kV, and 30 mA). Raman spectra were recorded at different locations of the sample using a Jobin Yvon LabRam HR spectrometer with 632 nm Ar laser.

Electrochemical Characterizations: All the electrochemical analysis was performed using an electrochemical workstation (CHI760E and RRDE-3A, CH Instrument, USA) with a typical three-electrode system. Platinum coil was used as the counter electrode, Ag/AgCl (3M NaCl) as the reference electrode and Glassy carbon electrode (GCE, 3 mm diameter) was used as the working electrode. Prior to measurements, GCE was thoroughly polished with 1 μ , 0.3 μ and 0.05 μ alumina powder (CH Instruments Inc.) and subjected to N₂ flow for 30 minutes. For the preparation of working electrode 2 mg of the catalyst was ultrasonically dispersed in 300 μ L Nafion solution (Millipore water: Isopropanol: 5wt% nafion = 4 mL: 1 mL: 60 μ L) until homogenous dispersion was obtained. 10 μ L of this dispersion was carefully drop casted on the GCE and allowed to dry overnight under ambient atmosphere. Internal and solution iR_s drop within the cell was compensated for all the cathodically polarized curves. The electrolyte used was 0.5 M H₂SO₄ saturated with Ar gas flow for 30 minutes to remove the dissolved oxygen. During the measurement, flow of Ar was maintained on the headspace of electrolyte to minimize the disturbance due to gas purging. The working electrode was rotated at 1600 r.p.m. throughout the measurement to remove hydrogen gas bubbles formed at the catalyst surface. The catalyst was electrochemically washed between the potential range of 0.2 -0.9 V before the measurement. Linear Sweep Voltametry (LSV) was performed at 1600 rpm and scan rate of 5

mV/s. Electrochemical Impedance Spectroscopy (EIS) was done at the voltage corresponding to the onset potential of Hydrogen Evolution Reaction (HER). For testing the stability of the catalyst Chronopotentiometry (CP) and Chronoamperometry (CA) was performed at current density of 20 mA/cm² and overpotential (η) of -0.32 V respectively. All the measurements were done at room temperature.

Table S1: Composition and the sample names used in our experiment

Sample	Composition *	Boric acid (mg)	Activated Charcoal (mg)	Urea (g)
BCN-1	BC ₇ N ₂	60	500	2.4
BCN-2	BC ₄ N _{1.2}	60	250	2.4
BCN-3	BC _{1.7} N _{0.7}	60	150	2.4
BCN-4	BC _{1.7} N _{0.8}	30	250	2.4
BCN-5	BC _{1.1} N	30	150	2.4

* Also obtained from CHN elemental analysis.

Table S2: Relative percentage of different kinds of nitrogen present on the surface of the BCN samples

Sample	Type of Nitrogen and its percentage (%)			
	Pyridinic-N	Pyrrolic	Graphitic-N	Pyridinic-N oxide
BCN-1	78	3	19	--
BCN-2	74.5	25.5	--	--
BCN-3	54.5	45.5	--	--
BCN-4	52.8	35.2	--	11.8
BCN-5	56.6	--	--	43.4

Table S3: Relative percentage of B-C and B-N on the surface of the BCN samples

Sample	B-C (%)	B-N (%)
BCN-1	53.2	46.8
BCN-2	59.8	40.2
BCN-3	37.5	62.5
BCN-4	100	--
BCN-5	17.4	82.6

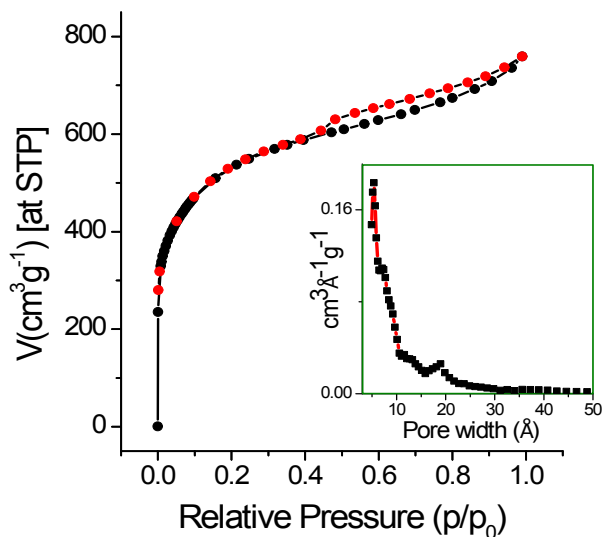


Fig. S1: BET adsorption isotherm of BCN-1 showing typical type-IV behavior consisting of mesopores. Inset shows the pore size distribution in BCN-1.

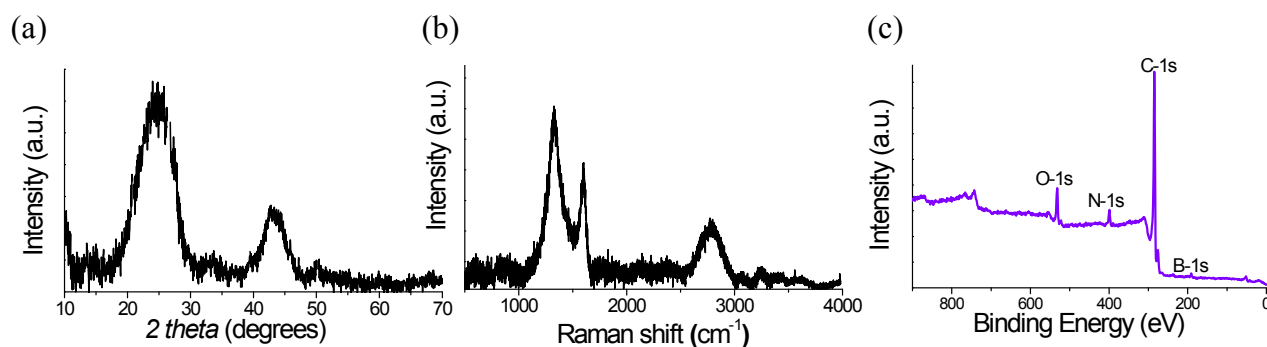


Fig. S2: (a) and (b) PXRD and Raman spectra of BCN-1. (c) XPS Survey scan for the elements in BCN-1.

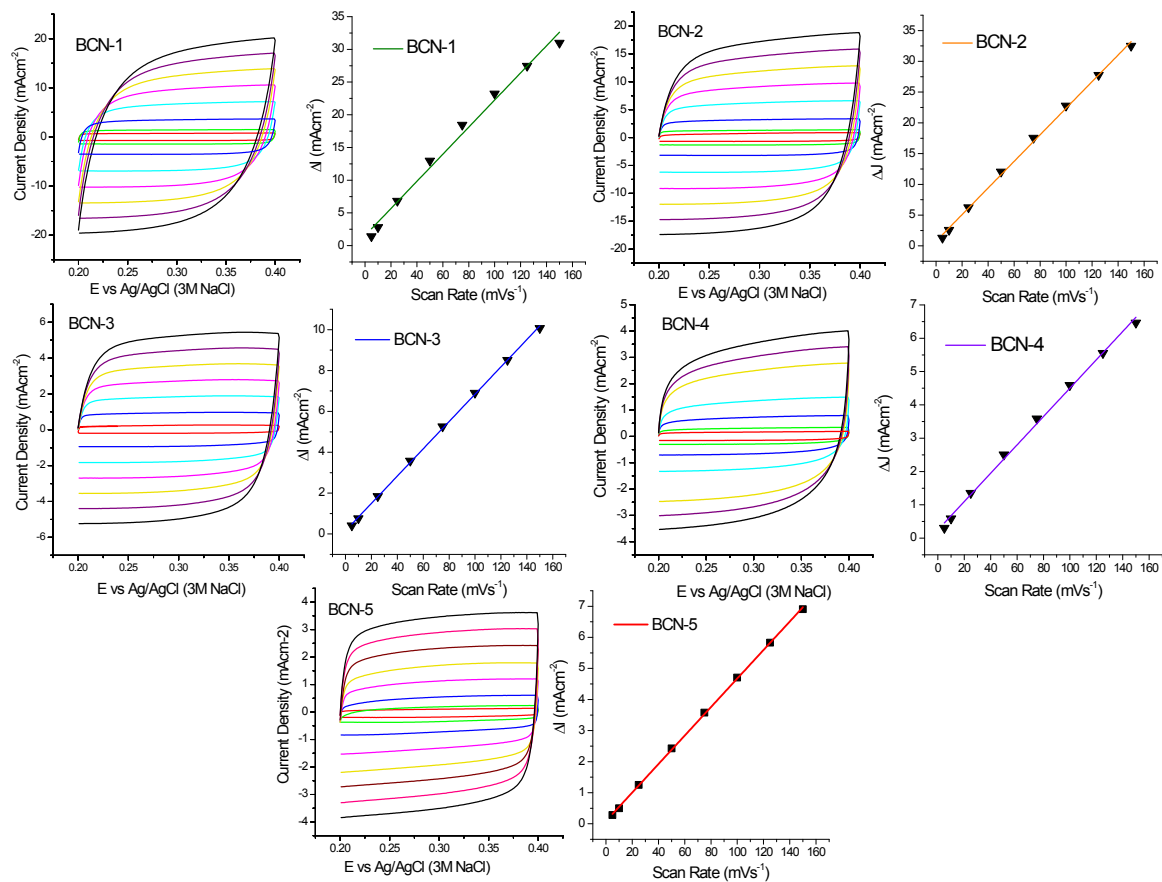


Fig. S3: (a, c, e, g, i) are the CV curves and (b, d, f, h, j) are the corresponding difference in the current density at 0.25 V plotted against scan rate to calculate the C_{dl} value from the slope after the linear fit.

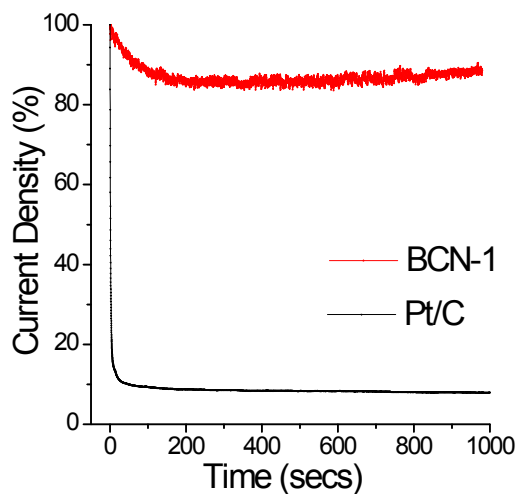


Fig. S4: Electrocatalytic HER activity retention comparison of BCN-1 with Pt/C. Data was collected from the chronoamperometric $i-t$ curve performed at -0.32 V for 1000 seconds.

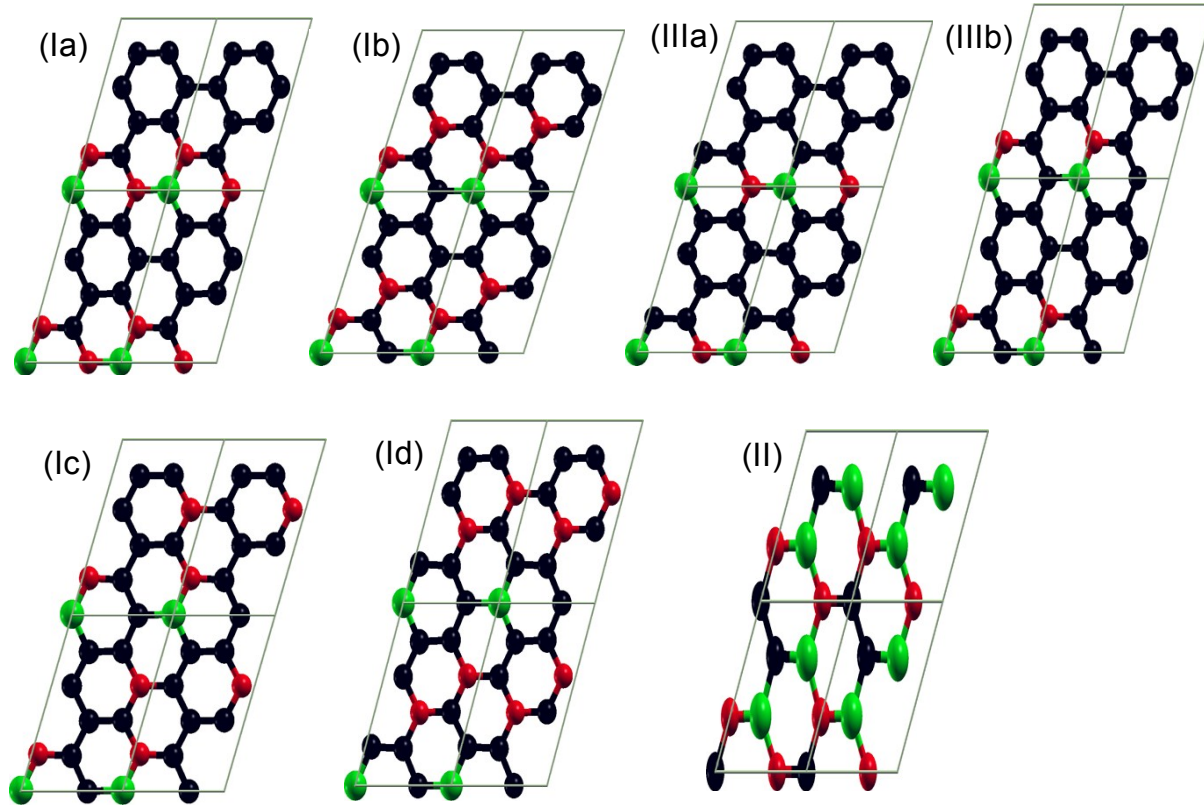


Fig S5: Schematics of three compositions (I, II and III), along with their symmetrically inequivalent configurations. C atoms are denoted by black, B by green and N by red.

Table S4: Comparison of valence band maxima, conduction band minima (VBM and CBM), E_F and DOS (E_F) of different configurations studied. For each composition (I, II and III), the relative energies of their configurations are mentioned with respect to the lowest energy configuration.

Configuration	Relative Energy $E(\text{config}) - E(\text{lowest})$ (eV/supercell)	VBM (eV)	CBM (eV)	E_F (eV)	DoS(E_F) (arb. units)
Ia	0	-4.888	-4.094	-2.934	1.747
Ib	1.076	-4.738	-4.341	-3.127	1.312
Ic	0.819	-4.976	-4.377	-3.086	1.143
Id	2.078	-4.830	-4.558	-3.171	1.193
II	-	-4.112	-3.595	-3.833	0
IIIa	0	-4.335	-3.832	-4.078	0
IIIb	0.132	-4.252	-3.966	-4.109	0

Calculation of double layer capacitance (C_{dl}):

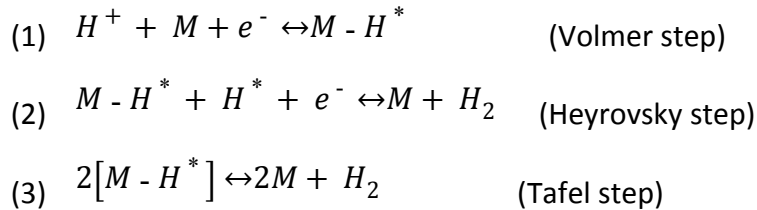
Since most of the electrochemical activities of the catalysts reported in literature for HER are either mass normalized or electrochemically active surface area normalized, we calculated the C_{dl} using a simple CV method. And the value of C_{dl} is linearly proportional to the electrochemically active surface area of the electrode. A potential range of 0.2-0.4 V was selected for the capacitance measurements because in this potential window no faradaic process corresponding to HER occurs and the electrode can be expected to behave as an ideally polarizable electrode (IPE). The variation of current of such an electrode as a function of time when the measurement is done at a certain voltage ramp say ν V/s is given by²,

$$i = \nu C_d [1 - \exp(-t/R_s C_d)] \quad (3), \text{ where } R_s \text{ is the solution resistance.} \quad \nu C_d \text{ is}$$

the saturation current at large time. Thus plot of $\Delta I |i_a - i_c|$ at 0.25 V against scan rate ν gives a straight line with slope twice the value of C_{dl} .

Note on Tafel slope:

Electrochemical generation of hydrogen is generally multistep phenomenon on the surface of the catalyst. In acidic medium the reaction is believed to proceed through the following steps³.



where H^* is the chemically adsorbed hydrogen atom on the active site of catalyst (M). The first step (equation 1) is common step but then the evolution of hydrogen can proceed through any of the later two steps (equation 2 or 3). To find the probable pathway of H_2 generation tafel slope is generally employed. From the Butler Volmer equation, theoretically calculated tafel slope for Pt as a model catalyst should be 29 mV/dec assuming that the tafel step as the rate determining step (rds). If Heyrovsky step is the rds then tafel slope should be 38 mV/dec. however if the first step, discharge or the volmer step is slowest then irrespective of whether H_2 evolution takes place by later two steps, the tafel slope should be 116mV/dec^[3]. It should be noted that lower the value of tafel slope better is the catalyst for HER. In addition to this

exchange current density (i_0) is the vital depictor of catalysts' inherent activity. It is defined as the current density in one direction (cathodic or anodic) at an equilibrium potential of a reaction. It correlates the rate of electron transfer under reversible conditions with the overpotential. The tafel equation can be used to calculate the value of i_0 and charge transfer coefficient (α).

$$\eta = a + b \log(i/i_0) \quad (4), \quad \text{where} \quad 'b' = -\frac{2.303RT}{\alpha F} \quad \text{and is the tafel slope and}$$

$$'a' = \frac{2.303RT}{\alpha F} \log(i_0)$$

Methods of first principles calculations:

Our calculations are based on first-principles density functional theory (DFT) as implemented in the Quantum ESPRESSO code⁴. We use a generalized gradient approximation (GGA) with Perdew-Burke-Ernzerhof⁵ (PBE) parameterization of exchange correlation energy functional with ultrasoft pseudopotentials⁶. An energy cut off of 30 Ry was used for truncating the plane wave basis set to represent wave functions, and 240 Ry for the density. We use periodic boundary conditions with a supercell that keeps vacuum in the separation between periodic images of width 8 Å. The structures were relaxed till the magnitude of Hellman-Feynman force on each ions becomes smaller than 0.03 eV Å⁻¹. Brillouin zone integrations were carried out with a uniform 12 X 10 X 1 mesh of k -points.

We use first-principles density functional theoretical calculations to determine electronic structure and energetics of various compositions of carbon rich $B_xC_{1-x-y}N_y$ with a goal to understand their electrocatalytic activity in HER observed here. We focus on three compositions: BC_7N_2 (I), $B_2C_2N_2$ (II) and BC_8N (III) (see Fig. S5), which show great contrast in their electrocatalytic activity. We consider four symmetry inequivalent configurations of (I) obtained by replacing a carbon atom in the 10-atoms supercell of graphene (Fig. S5) with boron, and substituting two N atoms at different pairs of carbon sites (Fig. S5). Both N atoms are bonded to B atom in configurations (Ia), while only one of them is bonded to B in the other two configurations (Ib and Ic) and none of them in Id. Consistent with earlier work¹, the configurations,

1a has the lowest energy, followed by 1c, 1b and 1d (Table S4). Similarly, we considered one configuration of composition (II) and two configurations of composition (III) (Fig. S5).

Faradaic efficiency measurements

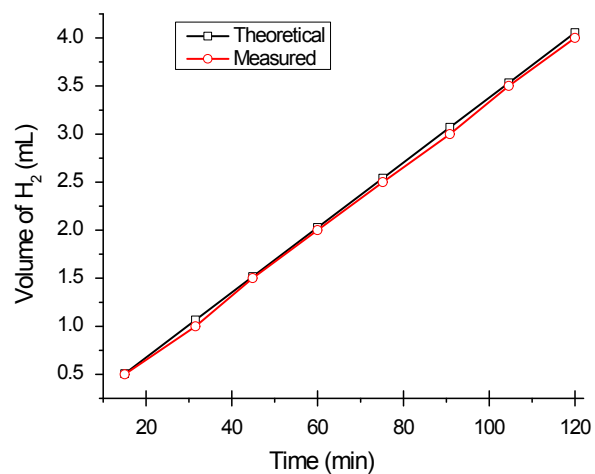


Fig. S6: Quantity of H₂ gas evolved as a function of time for BC₇N₂

Metal-free electrocatalyst for hydrogen evolution reaction

The presence of trace metal impurities will lead to abrupt change in the electrochemistry of the parent material. Recent studies have extensively revealed this fact that for carbon based “metal-free” electrocatalysts, if these trace amounts of metals (Fe, Ni, Co, Mn, Cr etc) are present in the sp² carbon nanomaterials, it leads to dramatic influence in the electrocatalytic activity especially in ORR. Hence it has become imperative to check its presence in “metal-free” catalysts (as has been argued by many researchers, *Chem. Commun.*, 2014, 50, 12662–12664; *Angew. Chem. Int. Ed.* 2013, 52, 13818–13821; *Angew. Chem. Int. Ed.* 2006, 45, 2533–2537). We selected 7 probable electrochemically active metal impurities (Pt, Fe, Mn, Co, Cr, Ni and Cu). We confirm the absence of these metal impurities [except Fe, 1.5 wt% (30.1 µg) in the catalyst ink] in our catalyst by ICP-AES. We tested BCN-1 and also the initial precursors-Boric acid, Urea and activated charcoal. The findings are detailed in table below. The effect of the presence of Fe on HER activity has been studied by introducing Fe into the BCN sample (3%, 6% and 9%). [BCN was ultrasonicated in FeCl₃ solution and was reduced by NaBH₄ to introduce Fe in the BCN]. There was no appreciable linear change in the onset potential seen due to presence of Fe. Hence we conclusively propose that the electrocatalytic HER activity of BCN is not due to the probable presence of trace metal impurities.

Table: Study of the presence of trace metal impurities in the catalyst ink and the initial precursors.

Sample	Pt (µg)	Fe(µg)	Mn(µg)	Cu(µg)	Ni(µg)	Co(µg)	Cr(µg)
H ₃ BO ₃ (in 60 mg)	8.6	12.2	13.6	13.3	13.3	8.6	24.7
Urea (in 2.4 g)	230	468	538	509.5	583.6	353	492
Act. Charcoal (in 500 mg)	5.6	81.8	14.0	3.9	14.4	8.5	24.1
BCN-1 (in 0.05 mg)	2.1 ng	30.1	5.7 ng	5.1 ng	0.9	3.4 ng	19.1ng

ng= nanograms. ; Mass of sample deposited on GCE is 0.05 mg.

Presence of oxygen functional group and its effect on HER activity

O-1s can be decomposed into three peaks corresponding to 530.2 eV, 532 eV, 533.6 eV which are respectively due to the presence of C=O, COOH and oxygen attached to the graphitic carbon with nitrogen in it. These functional groups help in effective doping of N and B by acting as a reactive site during the reaction. The presence of both oxygen and nitrogen where oxygen is bonded to nitrogen in the carbon ring has been shown to be electroactive than the oxygen devoid of nitrogen attachment in case of ORR (*J. Power sources*, 225 (2013) 192-199) but its activity is negligible in comparison to N. However the aim is to reduce these oxygen

functionalities from the carbon (tried by treatment with ammonia vapor in our case) moiety due to its negative effect in the conductivity of the electrocatalyst. Though oxygen is more electronegative than N and C, it is still not electroactive for HER in the form of the surface functional groups mentioned above. Unlike B and N it is not the part of sp^2 carbon rings and hence cannot contribute to the electron delocalization and faster electron transfer reactions. it may be noted that most heteroatom dopants using carbon based catalysts find oxygen on the

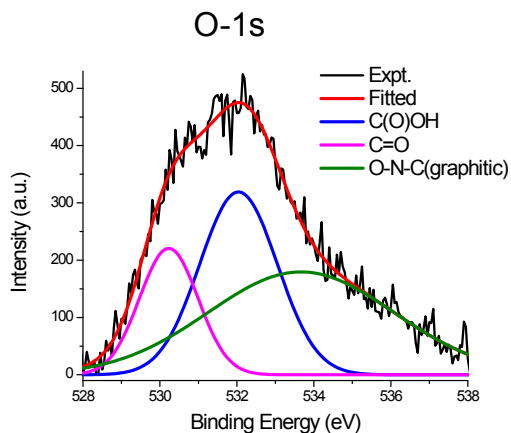


Fig. : X-ray photoelectron spectrum of BCN-1 showing core level spectrum of Oxygen.

surface, but donot discuss this aspect

Study of the catalytic HER performance of BC_7N_2 catalyst in basic medium

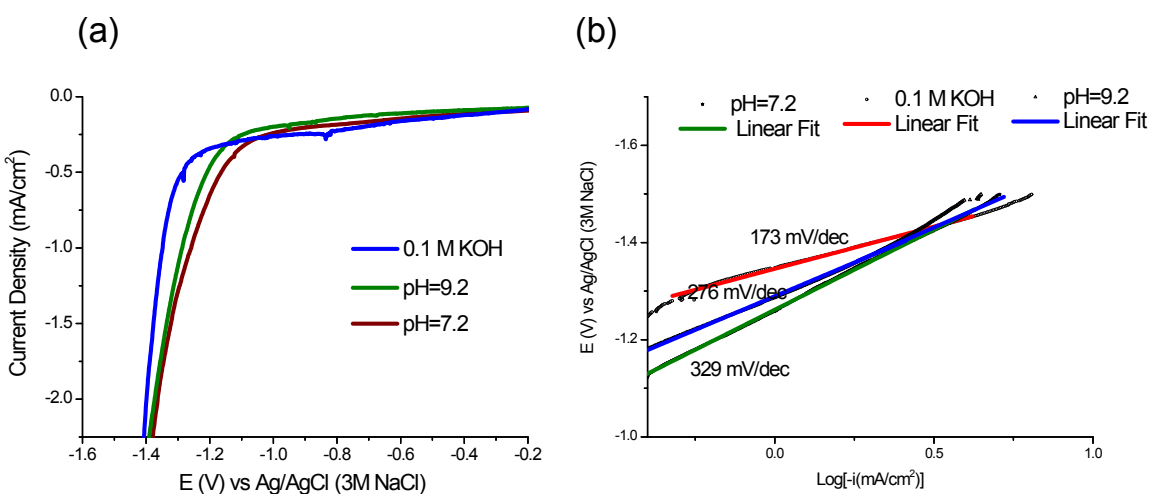


Fig.: (a) HER activity comparison of BC_7N_2 in three different pH of the electrolyte. (b) The Tafel slopes of BC_7N_2 in different pH of the electrolyte, as calculated from the LSV curves in (a).

The study of the effect of the presence of B and N in the BCN network in the electrochemical HER activity

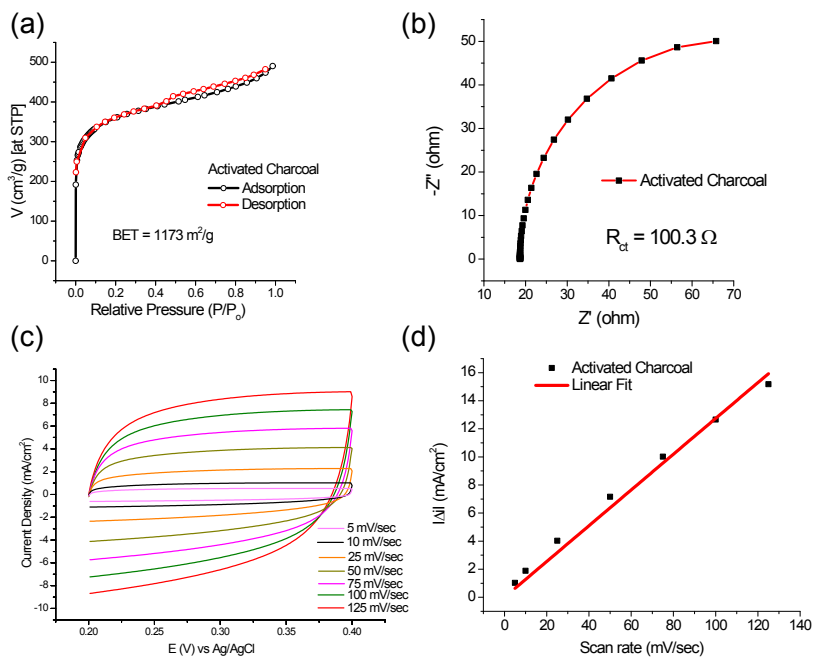


Fig. S8: (a) N_2 adsorption/desorption profile of activated charcoal (b) Nyquist plot of activated charcoal at the onset potential, (c) and (d) are respectively CV curves and the corresponding difference in the current density at 0.275 V plotted against scan rate to calculate the C_{dl} value from the slope after the linear fit.

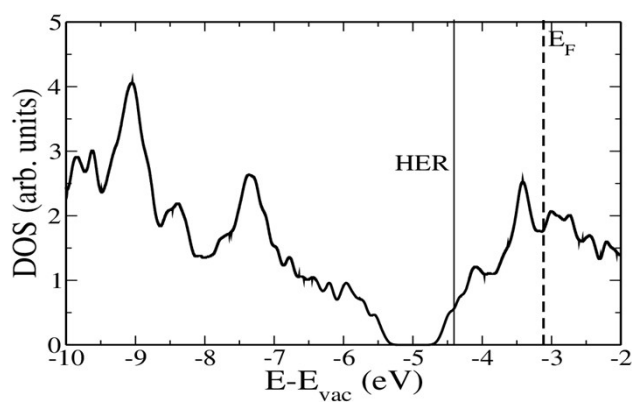


Fig. S9: DOS of C_8N_2

Study of the effect of configuration of BC₇N₂ in the adsorption of electrolyte.

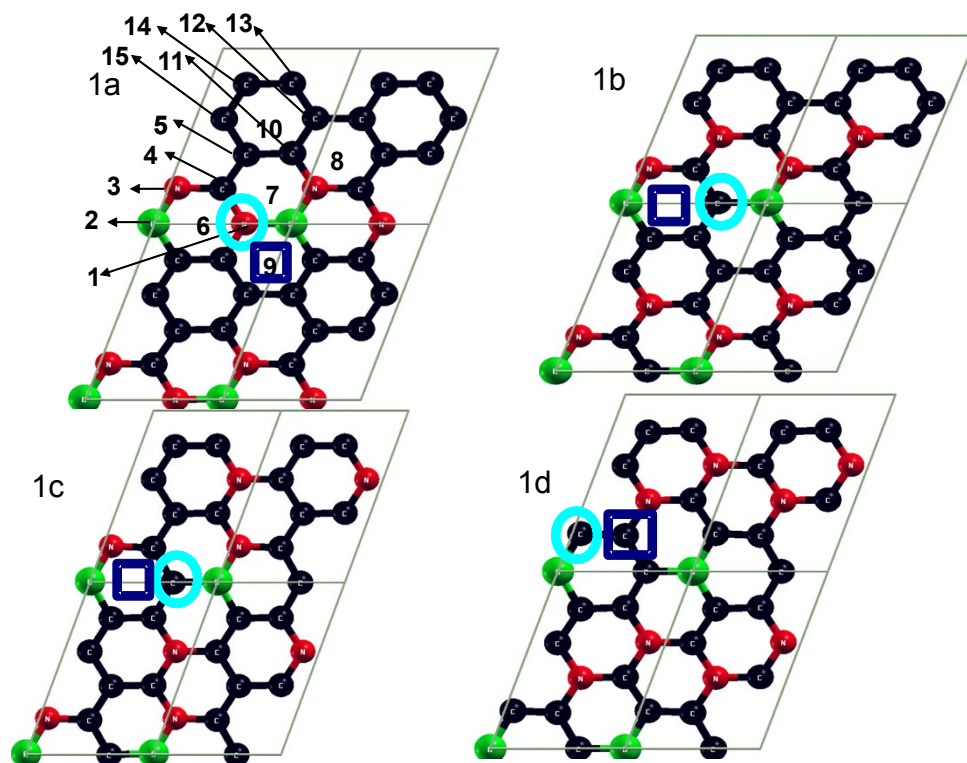


Fig S10: Different absorption sites of H₂O molecule in 1a (same for 1b, 1c and 1d configurations). The weakest and strongest absorption sites are marked by circles and squares respectively.

We present results of about 60 configurations to study interactions between H₂O and BC₇N₂ and their energetics (including van der Waals interactions) on 1a, 1b, 1c and 1d chemically ordered states of BC₇N₂ (see Fig S10). These configurations are obtained by considering different sites of adsorption of H₂O (O above the atoms (B, C and N), and above the centre of hexagonal rings), with the water molecule oriented parallel to the BC₇N₂ plane, at a distance of 1.4 Å. We find that their adsorption energies lie in the range of 11-28 kJ mol⁻¹ (see Fig S11). The weakest adsorption occurs when H₂O interacts with N site of 1a state, and it is the strongest at the centre of hexagonal rings for 1a and 1b states (see Fig S10).

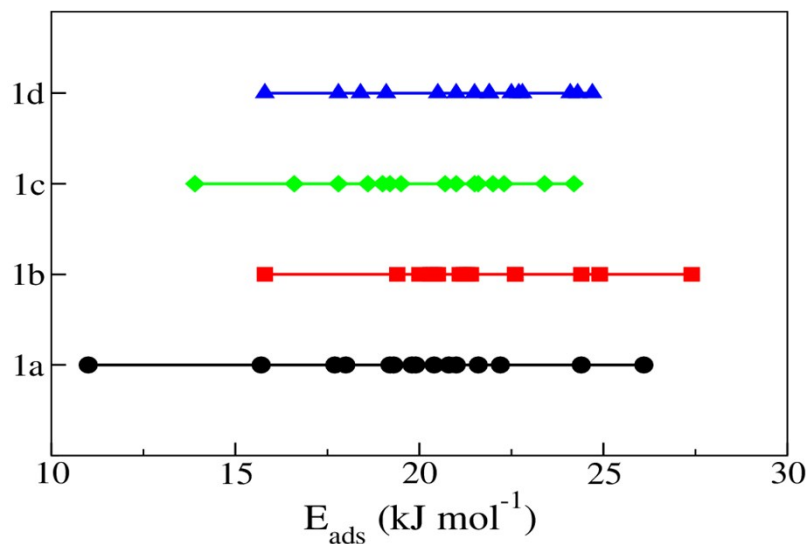


Fig S11: Comparison of the absorption energies at different adsorption sites for 1a–1d configurations of BC_7N_2 .

Study of the effect of BN and the CN domains on HER activity of $B_xC_yN_z$

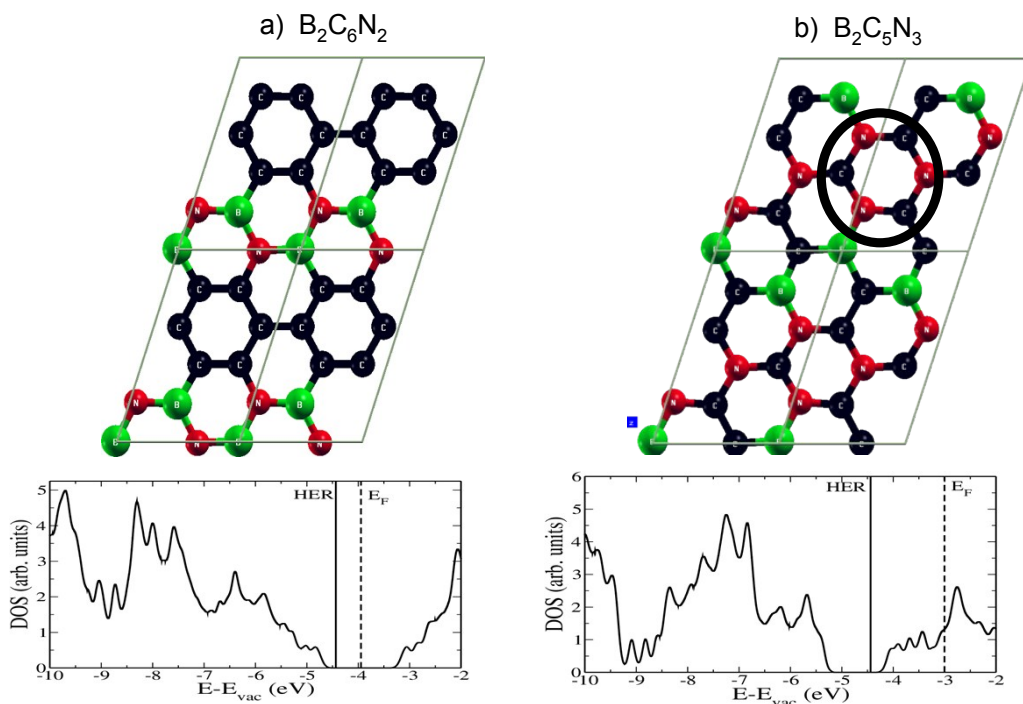


Fig. 12: Schematic of a) $B_2C_6N_2$, b) $B_2C_5N_3$ (C-N ring is marked by black circle) and their corresponding DOS

Stability

- $E(\text{B}_2\text{C}_6\text{N}_2) - 3E(\text{C}_2) - 2E(\text{BN})_2 = 1.96 \text{ eV}$
- $E(\text{B}_2\text{C}_3\text{N}_5) - E(\text{BC}_7\text{N}_2) - E(\text{BN}) + E(\text{C}_2) = 2.27 \text{ eV}$
- **Both $\text{B}_2\text{C}_6\text{N}_2$ and $\text{B}_2\text{C}_3\text{N}_5$ are energetically less stable.**

References:

- (1) N. Kumar, K. Moses, K. Pramoda, S. N. Shirodkar, A. K. Mishra, U. V. Waghmare, A. Sundaresan and C. N. R. Rao, *J. Mater. Chem. A*, 2013, **1**, 5806-5821.
- (2) Allen J bard, Larry Faulkner, *Fundamentals of Electrochemistry- Methods and Applications*. 2nd edition, Wiley, 2000.
- (3) Carlos G. Morales-Guio, Lucas-Alexandre Stern and Xile Hu *Chem. Soc. Rev.*, 2014, **43**, 6555-6569.
- (4) P. Giannozzi, S. Baroni, N. Bonini, M. Calandra, R. Car, C. Cavazzoni, D. Ceresoli, G. L. Chiarotti, M. Cococcioni, I. Dabo, A. Dal Corso, S. Fabris, G. Fratesi, S. de Gironcoli, R. Gebauer, U. Gerstmann, C. Gougoussis, A. Kokalj, M. Lazzeri, L. Martin-Samos, N. Marzari, F. Mauri, R. Mazzarello, S. Paolini, A. Pasquarello, L. Paulatto, C. Sbraccia, S. Scandolo, G. Sclauzero, A. P. Seitsonen, A. Smogunov, P. Umari, R. M. Wentzcovitch, *J. Phys. :Condens. Matter*, 2009, **21**, 395502.
- (5) J. P. Perdew, K. Burke and M. Ernzerhof, *Phys. Rev. Lett.*, 1996, **77**, 3865–3868.
- (6) D. Vanderbilt, *Phys. Rev. B: Condens. Matter Mater. Phys.*, 1990, **41**, 7892.